Geophysical Research Letters

RESEARCH LETTER
10.1029/2020GL088926

# Contrasting Transition Complexity Between El Niño and La Niña: Observations and CMIP5/6 Models

**Shih-Wei Fang**[1] and **Jin-Yi Yu**[1]

[1]Department of Earth System Science, University of California, Irvine, CA, USA

**Key Points:**
- El Niño transitions are dominated by, in order, episodic, cyclic, and multiyear patterns, but the reversed order is found for La Niña
- This asymmetry is caused by a subtropical Pacific mechanism that produces more episodic (multiyear) transitions for El Niño (La Niña)
- CMIP5 models fail to simulate the asymmetry due to a cold bias in their tropical mean states and an overly weak subtropical mechanism

**Supporting Information:**
- Supporting Information S1

**Correspondence to:**
J.-Y. Yu,
jyyu@uci.edu

**Citation:**
Fang, S.-W., & Yu, J.-Y. (2020). Contrasting transition complexity between El Niño and La Niña: Observations and CMIP5/6 models. *Geophysical Research Letters*, *47*, e2020GL088926. https://doi.org/10.1029/2020GL088926

Received 20 MAY 2020
Accepted 12 JUL 2020
Accepted article online 29 JUL 2020

**Abstract** The observed El Niño and La Niña exhibit different complexities in their event-to-event transition patterns. The El Niño is dominated in order by episodic, cyclic, and multiyear transitions, but the reversed order is found in the La Niña. A subtropical Pacific onset mechanism is used to explain this difference. This mechanism triggers El Niño/La Niña events via subtropical processes and is responsible for producing multiyear and episodic transitions. Its nonlinear responses to the tropical Pacific mean state result in more multiyear transitions for La Niña than El Niño and more episodic transitions for El Niño than La Niña. The CMIP5/6 models realistically simulate the observed transition complexity of El Niño but fail to simulate the transition complexity of La Niña. This deficiency in CMIP5 models arises from a weaker than observed subtropical onset mechanism and a cold bias in the tropical Pacific mean sea surface temperatures in the models.

**Plain Language Summary** A new asymmetry is found between the warm (i.e., El Niño) and cold (i.e., La Niña) phases of El Niño-Southern Oscillation (ENSO) in their event-to-event transition patterns. The observed El Niño transitions is dominated in order by the episodic, cyclic, and multiyear patterns, but the reversed order is found in the La Niña transitions. This difference in the transitions arises from a subtropical Pacific forcing mechanism that triggers ENSO events. The subtropical onset mechanism is found to generate more episodic transitions for El Niño than La Niña and more multiyear transitions for La Niña than El Niño. This asymmetry is due to nonlinear responses of the subtropical mechanism to the tropical mean sea surface temperatures (SSTs). State-of-art global climate models realistically simulate the observed transition complexity of El Niño but fail to reproduce the transition complexity of La Niña. This deficiency arises from a weak subtropical onset mechanism and a cold bias in the tropical Pacific mean SSTs in the models.

## 1. Introduction

El Niño-Southern Oscillation (ENSO) is a complex phenomenon that involves wide ranges of different patterns, amplitudes, and temporal evolutions (Capotondi et al., 2015; Kao & Yu, 2009; Timmermann et al., 2018; C. Wang et al., 2017; Yu & Fang, 2018; Yu et al., 2017). One important part of the complexity appears in the way that one ENSO event transitions to another. An El Niño (La Niña) event can be preceded by a La Niña (El Niño) event to result in a cyclic transition, by another El Niño (La Niña) event to become a multiyear transition, or by a neutral (non-ENSO) condition to become an episodic transition (Yu & Fang, 2018). ENSO onset mechanisms control how anomalies in sea surface temperature (SST) are established in the equatorial Pacific and play critical roles in controlling transition patterns (B. Wang et al., 2019; Yu & Fang, 2018).

Two primary onset mechanisms of ENSO have been identified: a tropical Pacific onset (TP-onset) mechanism and a subtropical Pacific onset (SP-onset) mechanism (C. Wang et al., 2017; Yu & Fang, 2018; Yu et al., 2017). The TP-onset mechanism invokes equatorial thermocline variations to initiate the SST anomalies associated with ENSO, such as those described by the recharged oscillator (Jin, 1997; Wyrtki, 1975) and delayed oscillator theories (Battisti & Anthony, 1989; Suarez & Schopf, 1988; Zebiak & Cane, 1987). This mechanism typically produces ENSO SST anomalies first in the eastern equatorial Pacific, where the thermocline is the shallowest and SSTs are most sensitive to thermocline variations. Yu and Fang (2018) find that the TP-onset mechanism generates mostly the cyclic transition and contributes to reduce ENSO transition complexity (ETC), although some complexity may arise from its asymmetric responses to El Niño and La Niña (Hu et al., 2017).

**Table 1**
*Classification of ENSO Transitions and Their Calendar Onset Months During the Analysis Period (1948–2016)*

| El Niño | Transition | Onset (Mon) | La Niña | Transition | Onset (Mon) |
|---|---|---|---|---|---|
| 1951 | Cyclic | 6 | 1949 | Episodic | 9 |
| 1957 | Cyclic | 4 | 1954 | Episodic | 5 |
| 1963 | Episodic | 6 | 1955 | Multiyear | 2 |
| 1965 | Cyclic | 5 | 1956 | Multiyear | 6 |
| 1968 | Episodic | 10 | 1964 | Cyclic | 4 |
| 1969 | Multiyear | 8 | 1970 | Cyclic | 6 |
| 1972 | Cyclic | 5 | 1973 | Cyclic | 5 |
| 1976 | Cyclic | 8 | 1975 | Multiyear | 3 |
| 1977 | Multiyear | 8 | 1983 | Cyclic | 9 |
| 1982 | Episodic | 4 | 1984 | Multiyear | 9 |
| 1986 | Episodic | 8 | 1988 | Cyclic | 4 |
| 1991 | Episodic | 9 | 1995 | Cyclic | 8 |
| 1994 | Episodic | 8 | 1998 | Cyclic | 6 |
| 1997 | Episodic | 4 | 1999 | Multiyear | 8 |
| 2002 | Episodic | 6 | 2000 | Multiyear | 9 |
| 2009 | Cyclic | 7 | 2007 | Episodic | 7 |
| 2015 | Episodic | 3 | 2008 | Multiyear | 10 |
| | | | 2010 | Cyclic | 5 |
| | | | 2011 | Multiyear | 7 |

On the other hand, the SP-onset mechanism invokes subtropical Pacific processes to trigger ENSO events (Yu et al., 2010; Yu & Kim, 2011). The subtropical processes include those described by the seasonal footprinting mechanism (Alexander et al., 2010; Kao & Yu, 2009; Vimont et al., 2003), trade wind charging (Anderson & Perez, 2015; Anderson et al., 2013), wind-evaporation-SST feedback (Xie & Philander, 1994), and Pacific meridional mode (PMM; Chiang & Vimont, 2004). This mechanism typically results in ENSO SST anomalies that first appear in the central equatorial Pacific, where the northeastern Pacific trade winds approach the equator (Yu et al., 2010). Yu and Fang (2018) find that the SP-onset mechanism can result in all three transition patterns and is a key source of ETC.

Recent studies (Fang & Yu, 2020; Yu & Fang, 2018) reveal that the SP-onset mechanism can be activated by both the warm (i.e., El Niño) and cold (i.e., La Niña) phases of the ENSO. However, the way that the SP-onset mechanism responds to the El Niño is not symmetric to its response to the La Niña. For example, it is relatively easy for a La Niña event to activate the negative phase of SP-onset mechanism and result in another La Niña, but it is not easy for an El Niño event to activate the positive phase of SP-onset mechanism and result in another El Niño. Therefore, it is possible that transition complexity can be different between these two ENSO phases. The goals of this study are to compare the transition complexity between El Niño and La Niña in the observations and to examine whether the CMIP5/6 models can reproduce the observed complexities, and, if not, to identify model deficiencies and their causes.

## 2. Data Sets and Methods

Monthly mean values of SST, surface wind, and sea surface heights (SSHs) were regridded to a common grid of 1.5° longitude by 1° latitude for analysis. The anomalies were defined as the deviations from the seasonal cycles (calculated from the analysis period 1948–2016) with their linear trends removed. The SST, surface wind, and SSH data are downloaded, respectively, from the Hadley Center Sea Ice and Sea Surface Temperature data set (HadISST) (Rayner et al., 2003), the National Centers for Environmental Prediction-National Center for Atmospheric Research (NCEP-NCAR) reanalysis (Kalnay et al., 1996), and the German contribution of the Estimating the Circulation and Climate of the Ocean project (Köhl, 2015). The same procedures were applied to the last 100 years of the preindustrial simulations produced by 34 CMIP5 models (Taylor et al., 2012; see Table S1 in the supporting information for the details of the models) and 20 CMIP6 models (Eyring et al., 2016; see Table S2). A TP-onset index and a SP-onset index were constructed from the combined SST, surface wind, and SSH anomalies using a multivariate empirical orthogonal function analysis (Xue et al., 2000; Yu & Fang, 2018; see Text S1 for details).

Using only the SST information, we identify the transition pattern (i.e., cyclic, multiyear, or episodic) for every El Niño and La Niña event based on the ENSO condition during the previous year (Figure S1; see Text S2 for detailed descriptions). For example, if an El Niño event is preceded by a La Niña condition during its previous year, we consider that El Niño event to be a cyclic transition event. Table 1 lists the transition pattern and onset calendar month of all El Niño and La Niña events during the analysis period. The same classification methodology is also applied to the CMIP5/6 model simulations.

## 3. Results

Figure 1a shows that, during the analysis period of 1948–2016, El Niño events are dominated by episodic transitions (52.9%; nine events), followed by cyclic transitions (35.3%; six events) and the least by multiyear transitions (11.8%; two events). However, La Niña events have a distinct dominance, where the percentages of multiyear (42.1%; eight events) and cyclic (42.1%; eight events) transitions are the most and episodic transitions become the least (15.8%; three events). The El Niño has the most percentage for episodic transitions and the least for multiyear transitions, whereas the La Niña has, reversely, the most percentage for multiyear

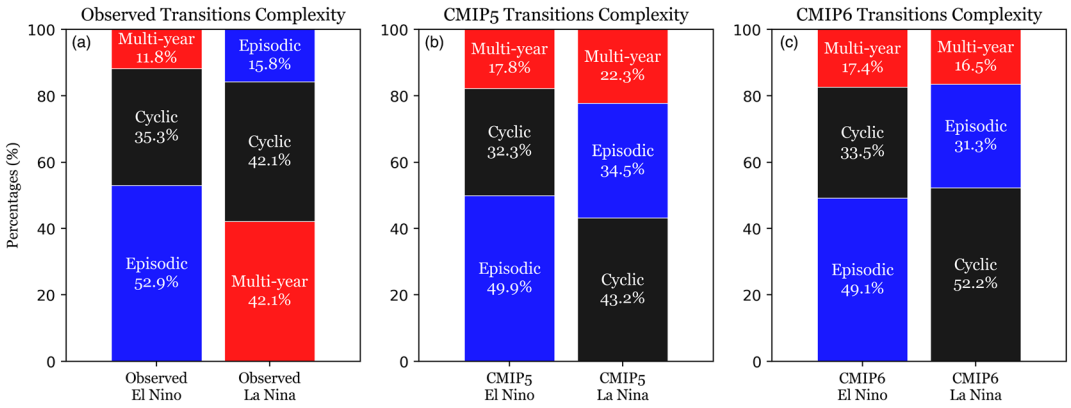


**Figure 1.** The transition complexity of El Niño (left bars) and La Niña (right bars) in (a) the observations, (b) the multimodel mean from 34 CMIP5 models, and (c) the multimodel mean from 20 CMIP6 models. The percentages of the transitions are ordered from highest (bottom) to lowest (top).

transitions and the least for episodic transitions. The transition complexity is thus asymmetric between the El Niño and La Niña phases of the ENSO. The asymmetry comes from the very distinct dominances of the episodic and multiyear transitions, while the cyclic transition accounts for similar percentages in El Niño and La Niña.

To understand the cause of the asymmetry, we contrast the evolutions of equatorial (5°S to 5°N) SST anomalies composited for the three transition patterns of El Niño and La Niña (Figures 2a–2f). As expected, ENSO SST anomalies in the cyclic, episodic, and multiyear transitions were preceded by opposite-signed, near-neutral, and same-signed anomalies in the previous year, respectively. It is important to note that the onset locations (during months −3 to 0) of the ENSO SST anomalies are different. The anomalies first appear in the eastern equatorial Pacific for both the cyclic El Niño and La Niña and in the central equatorial Pacific for both the multiyear El Niño and La Niña, whereas the SST anomalies show up in the central equatorial Pacific for the episodic El Niño but in the eastern equatorial Pacific for the episodic La Niña.

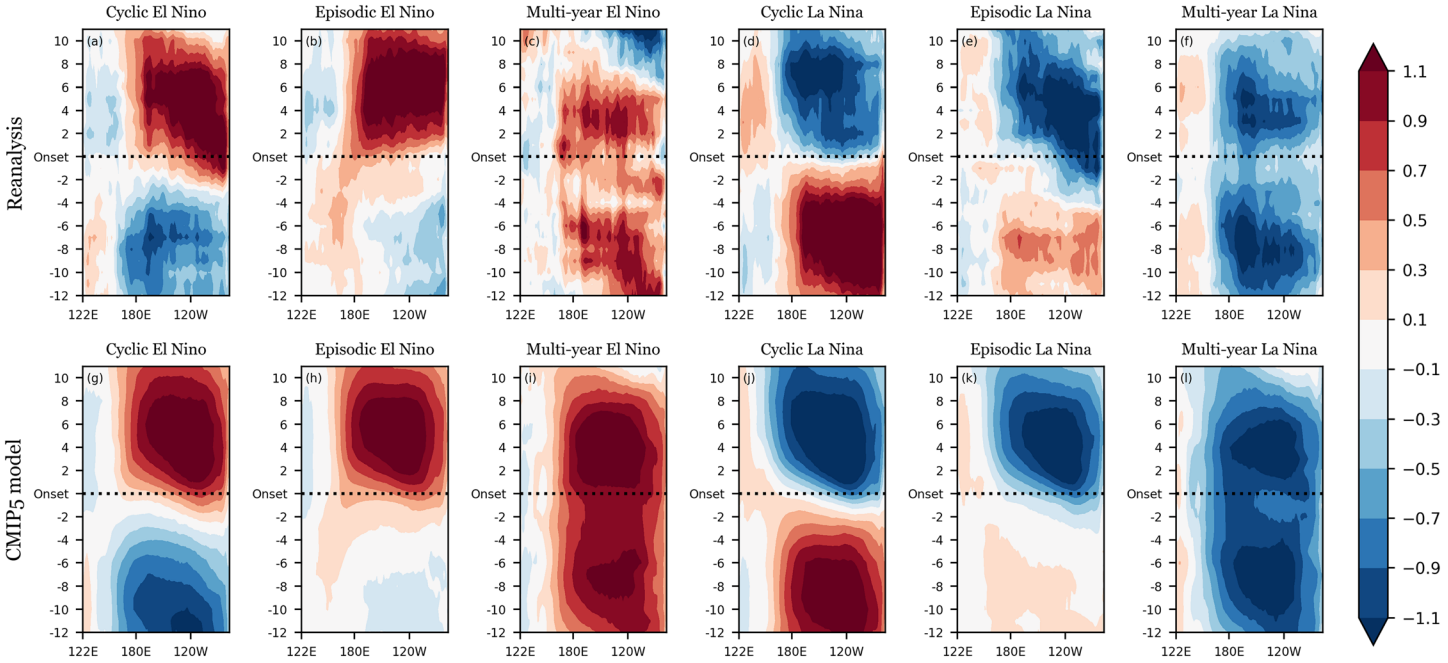


**Figure 2.** Evolutions of equatorial (5°S to 5°N) Pacific SST anomalies composited for the cyclic, episodic, and multiyear transitions of (a–c) El Niño and (d–f) La Niña in the reanalysis and (g–i) for the simulated El Niños and (j–l) La Niñas in the multimodel mean of CMIP5 simulations. The events are composited based on their onset time. Shadings are SST anomalies from 12 months before the ENSO onset month to 12 months after.

As mentioned, the TP-onset mechanism triggers ENSO events in which anomalies appear first in the eastern equatorial Pacific, whereas the SP-onset mechanism triggers ENSO events in which anomalies appear first in the central equatorial Pacific. The locations of SST anomalies in Figures 2a–2f suggest that the onset mechanisms are the same for the cyclic transition (the TP-onset mechanism) and multiyear transition (the SP-onset mechanism) of El Niño and La Niña but are different for the episodic El Niño and La Niña. While the SP-onset mechanism is more associated with the episodic El Niño, the TP-onset mechanism is more associated with the episodic La Niña. The values of the TP- and SP-onset indices during the onset period of each transition (see months −3 to 0 in Figures S1a–S1f) confirm this. Therefore, the causes of the asymmetric transition complexity are related to how these different mechanisms result in more frequent episodic El Niños than episodic La Niñas and how the SP-onset mechanism results in more multiyear La Niñas than El Niños.

Figure 2e shows that the episodic La Niña is preceded by weak warming. This evolution pattern is similar to that of the cyclic La Niña, except that in the episodic La Niña, the warming is not strong enough to be classified as an El Niño. Their associated thermocline evolutions (represented by the SSH anomalies; Figures S4d and S4e) are both characterized by a graduate shallowing of the thermocline depth during the preceding year. This indicates that the weak SST warming in the previous year discharges the equatorial Pacific to onset the La Niña. This confirms the contribution of the TP-onset mechanism to the episodic La Niña. On the other hand, one third of episodic El Niño events are also more associated with the TP-onset mechanism (Figures S5e and S5f), even though the majority of episodic El Niños are associated with the SP-onset mechanism. These results indicate that the TP-onset mechanism can generate both episodic El Niños and La Niñas but the episodic El Niño can also be additionally produced by the SP-onset mechanism. The fact that the SP-onset mechanism favors to produce episodic El Niños but not La Niñas can explain why episodic events account for a larger percentage of El Niños (52.9%) than La Niñas (15.8%).

Previous studies have shown that the SP-onset mechanism is more capable of producing episodic El Niño events than episodic La Niña events (e.g., Larson & Kirtman, 2013). One explanation for this is that an anomalous warming in the central equatorial Pacific can excite a stronger atmospheric feedback and more westerly winds than an anomalous cooling that induces easterly winds in the same region (Chen & Majda, 2016; Chen et al., 2019). Therefore, the initial warming triggered by the SP-onset mechanism in the central equatorial Pacific has a larger chance to develop into an episodic El Niño, but the initial equatorial cooling triggered by the SP-onset mechanism has a smaller chance to develop into an episodic La Niña.

As for the reason why the SP-onset mechanism produces more multiyear La Niñas than multiyear El Niños, Fang and Yu (2020) have offered an explanation. They find the occurrence frequencies of the multiyear El Niño and La Niña are controlled by the mean SSTs in the central equatorial Pacific. With a mean SST there that is slightly higher than the threshold temperature (28°C) for deep convection, a La Niña cooling in the region can abruptly turn off the deep convection. This generates a strong heating anomaly that excites a stronger wave train response than a comparable El Niño warming in this region (Fang & Yu, 2020; Lyu et al., 2017; Stuecker, 2018). The stronger (weaker) wave train response is more (less) capable of activating the SP-onset mechanism and to onset another La Niña (El Niño) in the following year. Therefore, present-day mean SSTs in the equatorial Pacific favor more multiyear La Niña transitions than multiyear El Niño transitions.

We next examine whether CMIP5 models can simulate the differences in transition frequencies between El Niño and La Niña described above. Preindustrial simulations produced by 34 CMIP5 models were analyzed (Table S1). Their multimodel means (MMMs) (Figure 1b) show that the simulated El Niño has a similar transition complexity as in the observations. Episodic El Niño transitions account for the highest percentage (49.93%), followed by cyclic El Niño transition (32.27%), with multiyear El Niño transitions least frequent (17.80%). However, the CMIP5 models cannot reproduce the observed frequency of occurrence of the La Niña transition patterns. While the multiyear La Niña transition accounts for the highest observed percentage, it accounts for the least of the simulated La Niña transitions (22.3%). The leading transition pattern for the simulated La Niña is the cyclic transition (43.18%), followed by the episodic transition (34.5%).

We further examine the transition complexity in each individual CMIP5 model and present the results using an ETC diagram (Figure 3). In the diagram, the *x*- and *y*-axis values are, respectively, the percentages of episodic and multiyear transitions in each model. The percentage of cyclic transitions, which can be calculated

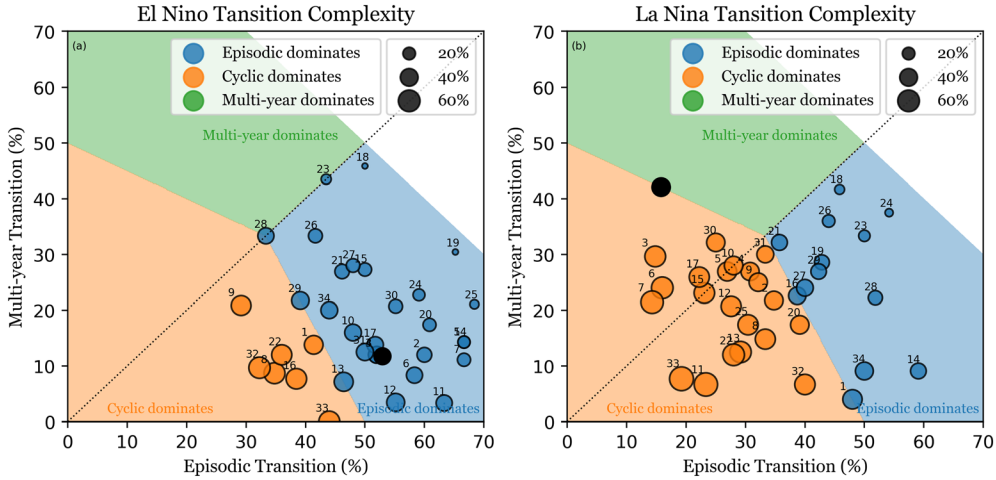


| | | | | | | |
|---|---|---|---|---|---|---|
| 1 :ACCESS1-0 | 6 :CESM1-FASTCHEM | 11:CNRM-CM5 | 16:GISS-E2-R | 21:IPSL-CM5A-MR | 26:MPI-ESM-LR | 31:NorESM1-ME |
| 2 :ACCESS1-3 | 7 :CESM1-WACCM | 12:CNRM-CM5-2 | 17:GISS-E2-R-CC | 22:IPSL-CM5B-LR | 27:MPI-ESM-MR | 32:bcc-csm1-1 |
| 3 :CCSM4 | 8 :CMCC-CESM | 13:CanESM2 | 18:HadGEM2-CC | 23:MIROC-ESM | 28:MPI-ESM-P | 33:bcc-csm1-1-m |
| 4 :CESM1-BGC | 9 :CMCC-CM | 14:GFDL-ESM2G | 19:HadGEM2-ES | 24:MIROC-ESM-CHEM | 29:MRI-CGCM3 | 34:inmcm4 |
| 5 :CESM1-CAM5 | 10:CMCC-CMS | 15:GFDL-ESM2M | 20:IPSL-CM5A-LR | 25:MIROC5 | 30:NorESM1-M | |

**Figure 3.** ENSO transition complexity (ETC) diagrams for (a) the simulated El Niño and (b) the La Niña in CMIP5 models in CMIP5 models. The *x* and *y* axes are, respectively, the percentage of episodic transitions and multiyear transitions in each model. The size of the circles is proportional to the percentage of cyclic transitions. The color of the circle indicates the highest percentage of transitions: Orange for cyclic, blue for episodic, and green for multiyear transition. The same color scheme is used in the background shadings to indicate the regions of the diagram where each of the three transitions is most frequent. The black dot is the observations, and the CMIP5 models are labeled with their corresponding numbers.

as "100 − (*x*-axis value + *y*-axis values)," is represented by the circle size (larger dots for higher percentages). Based on all possible values on the *x* and *y* axes, we can divide the ETC diagram into regions where cyclic, episodic, or multiyear transition has the largest percentage and dominates the transitions. Figure 3a shows that all but two CMIP5 models realistically produce more episodic El Niños than multiyear El Niños (i.e., below the dashed line of $x = y$) and that all but seven models have El Niño transitions that are dominated by the episodic type. The observed transition complexity of El Niños is realistically reproduced in most of the CMIP5 models.

The ETC diagram for La Niña (Figure 3b) reveals which transitions are responsible for the model deficiency. Only five CMIP5 models produce more multiyear La Niñas than episodic La Niñas (i.e., above the dashed line of $x = y$), and no model has La Niña transitions that are dominated by multiyear transitions. The CMIP5 models have a tendency to simulate too many episodic La Niñas and too few multiyear La Niñas, failing to reproduce the observed transition complexity of La Niña.

To identify the sources of these model deficiencies, we examine the MMM evolutions of the equatorial SST anomalies during the three transitions (Figures 2g–2l). Overall, all three transitions for the simulated El Niño and La Niña have onset locations similar to those in the observations. This similarity implies that the underlying transition dynamics in the models are similar to those in the observations. The relative strengths of the TP- and the SP-onset indices in the models also confirm this assertion (Figure S2). The SP-onset index is relatively stronger than the TP-onset index in the episodic El Niño, multiyear El Niño, and multiyear La Niña. In contrast, the TP-onset index is relatively stronger than the SP-onset index in the episodic La Niña, cyclic El Niño, and cyclic La Niña. However, we notice that the episodic El Niños in the models also show an onset signature in the eastern equatorial Pacific, which is absent in the observations. This difference suggests that the models have an overly strong TP-onset mechanism. We find that in about half of the CMIP5 models (16/34), the episodic El Niño is more associated with the TP-onset mechanism (Figures S6e and S6f). This is consistent with Yu and Fang (2018), who find most CMIP5 models have stronger than observed TP-onset mechanisms and weaker than observed SP-onset mechanisms. Since the episodic El Niño can be generated by both mechanisms, the frequency of occurrence of the episodic El Niño in the models may not be much different from observations in spite of the weaknesses noted in the

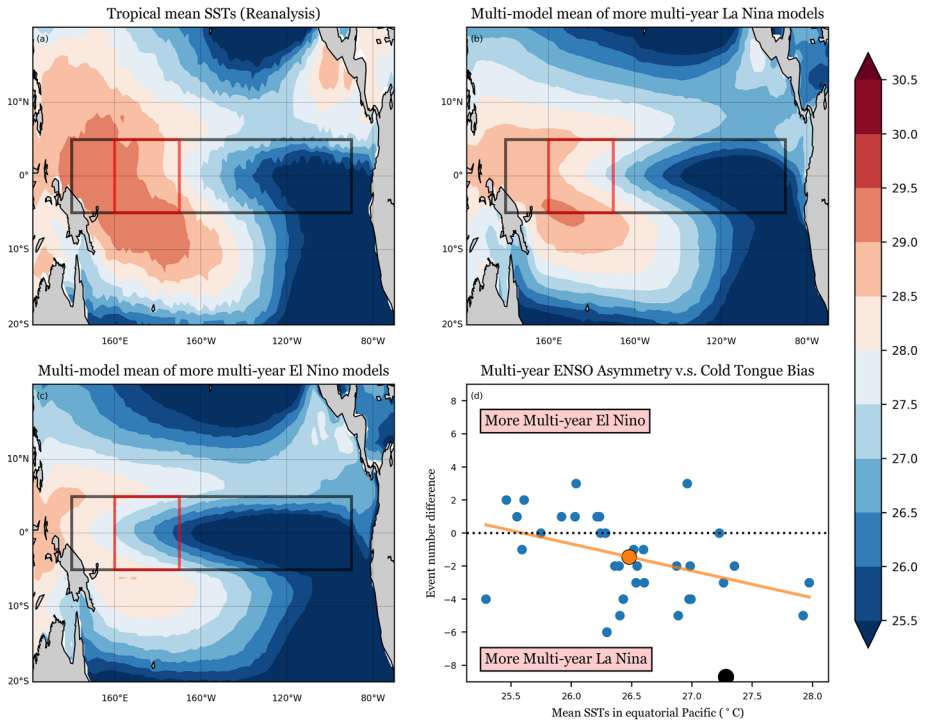


**Figure 4.** (a) Mean SSTs in the tropical Pacific calculated from (a) the observations during 1948–2016, (b) the five CMIP5 models with the most multiyear El Niños in Figure S7, and (c) the five CMIP5 models with the most multiyear La Niñas. The red box denotes the equatorial central Pacific region (5°S to 5°N and 160°E to 170°W). Panel (d) displays the relationship between the event number difference and the mean SST across the equatorial Pacific (5°S to 5°N and 140°E to 120°W; the black box). The black dot is the reanalysis value (scaled to event numbers in 100 years as in model simulation), and the orange dot is the multimodel mean value with the orange line representing the linear regression (passing 99% significance test).

simulations of the two onset mechanisms. In contrast, the episodic La Niña is produced primarily by the TP-onset mechanism, leading to an overestimation of episodic La Niña events in the models (34.5% vs. 15.8% in the observations).

The recent study of Fang and Yu (2020) has suggested that the slightly above 28°C mean SST in the central equatorial Pacific is a reason why the SP-onset mechanism produces more multiyear La Niñas than multiyear El Niños in the observations. Our finding that the CMIP5 models produce a smaller asymmetry between the numbers of multiyear El Niños and La Niñas (22.3% vs. 17.8%; see Figure 1b) implies that the mean SSTs in the models are different from the observations. To examine this possibility, we contrast in Figure 4 the mean SSTs in the tropical Pacific between the five models that produce the most multiyear La Niñas and the five models that produce most multiyear El Niños (see Figure S7 for the models). The group with more multiyear La Niñas (Figure 4b) has mean SSTs that are similar to the observations (Figure 4a), slightly warmer than the 28°C in the central equatorial Pacific (red boxes in Figure 4). In contrast, the group with more multiyear El Niños (Figure 4c) shows much colder mean SSTs in the central equatorial Pacific (27.3°C). This is consistent with the suggestion of Fang and Yu (2020) that a warmer (colder) mean SST in the equatorial central Pacific favors more multiyear La Niña (El Niño) events.

Contemporary models are known to have a tendency to produce a lower than observed mean SSTs in the central equatorial Pacific associated with a cold tongue that extends further westward than observed (Davey et al., 2002; Li et al., 2016; Misra et al., 2008; Vannière et al., 2013). We therefore examine in Figure 4d the relationship between the model differences in multiyear transitions and the model mean SSTs across the equatorial Pacific (5°S to 5°N and 140°E to 120°W; black boxes in Figure 4). A significant (at 99% level) linear relationship exists between these two quantities. The colder the mean equatorial SSTs in the model, the stronger tendency to have more multiyear El Niños. The MMM value of the mean SST (26.5°C) is colder than the observed value (27.3°C), leading to the weaker tendency for more

multiyear La Niñas in the models. The well-known cold bias in the equatorial Pacific is a key reason why the CMIP5 models cannot reproduce the observed El Niño-La Niña asymmetry in multiyear transitions.

We repeated the analyses with 20 CMIP6 models (Figure S3) and obtained similar results (Figure 1c). The CMIP6 models do not show any significant improvement over CMIP5 models in the simulation of ETC. Similar to the CMIP5 models, the CMIP6 models also reproduce the observed transitions for El Niño but fail to reproduce the La Niña transitions (Figures 1c and S8). The three transition patterns and their associated onset mechanisms are also similar to the CMIP5 models (Figure S9). The TP-onset mechanism is overestimated in the CMIP6 models, while the SP-onset mechanism is underestimated (Figure S10). A similar but weaker relation exists between the cold tongue bias and the multiyear La Niña tendency in the CMIP6 models (Figures S11 and S12). This weaker tendency reveals that differences exist in the simulated ETC between the CMIP5 and CMIP6 models (e.g., distinct atmospheric responses in CMIP models), even though both sets of models fail to reproduce the observed transition complexity for La Niña.

## 4. Summary and Discussion

In this study, we find that there are more episodic El Niños than La Niñas and more multiyear La Niñas than El Niños in the observations. This difference is the result of the nonlinear characteristics of the SP-onset mechanism. Our findings further confirm the critical roles of the SP-onset mechanism in determining the ETC and the transition asymmetry between the El Niño and La Niña. We find that the CMIP5 and CMIP6 models can reproduce the transition complexity for El Niño but not for La Niña. The models tend to produce too many episodic La Niña events and too few multiyear La Niña events. We are able to link the former deficiency to a weaker than observed SP-onset mechanism in the CMIP5/6 models and the latter to a cold bias in mean state SSTs in the equatorial Pacific in the CMIP5 models. To achieve better simulations of ETC, further efforts are to improve the model deficiencies in simulating the SP-onset mechanism and mean SSTs in the equatorial Pacific.

## Data Availability Statement

The HadISST SST data were downloaded from their site (http://www.metoffice.gov.uk/hadobs/hadisst/data/download.html). The wind fields of NCEP/NCAR were obtained from NOAA (https://www.esrl.noaa.gov/psd/). The GECCO2 SSH data sets were downloaded from the Integrated Climate Data Center (https://icdc.cen.uni-hamburg.de/en/gecco2.html).

**Acknowledgments**

We thank two anonymous reviewers for their valuable comments. This research is supported by NSF's Climate and Large-scale Dynamics Program under Grant AGS-1833075. We acknowledge the World Climate Research Programme's Working Group on Coupled Modelling, which is responsible for CMIP, and we thank the climate modeling groups, listed in Table S1 for CMIP5 (Taylor et al., 2012) and Table S2 for CMIP6 (Eyring et al., 2016), for producing and making available their model output. For CMIP the U.S. Department of Energy's Program for Climate Model Diagnosis and Intercomparison provides coordinating support and led the development of the software infrastructure in partnership with the Global Organization for Earth System Science Portals.

## References

Alexander, M. A., Vimont, D. J., Chang, P., & Scott, J. D. (2010). The impact of extratropical atmospheric variability on ENSO: Testing the seasonal footprinting mechanism using coupled model experiments. *Journal of Climate*, *23*(11), 2885–2901.

Anderson, B. T., & Perez, R. C. (2015). ENSO and non-ENSO induced charging and discharging of the equatorial Pacific. *Climate Dynamics*, *45*(9–10), 2309–2327.

Anderson, B. T., Perez, R. C., & Karspeck, A. (2013). Triggering of El Niño onset through trade wind-induced charging of the equatorial Pacific. *Geophysical Research Letters*, *40*, 1212–1216. https://doi.org/10.1002/grl.50200

Battisti, D. S., & Anthony, C. H. (1989). Interannual variability in a tropical atmosphere-ocean model: Influence of the basic state, ocean geometry and nonlinearity. *Journal of the Atmospheric Sciences*, *46*(12), 1687–1712.

Capotondi, A., Wittenberg, A. T., Newman, M., Di Lorenzo, E., Yu, J. Y., Braconnot, P., et al. (2015). Understanding ENSO diversity. *Bulletin of the American Meteorological Society*, *96*(6), 921–938.

Chen, N., & Majda, A. J. (2016). Simple dynamical models capturing the key features of the central Pacific El Niño. *Proceedings of the National Academy of Sciences*, *113*(42), 11,732–11,737.

Chen, N., Thual, S., & Stuecker, M. F. (2019). El Niño and the Southern Oscillation: Theory. In *Reference Module in Earth Systems and Environmental Sciences*. Elsevier. https://doi.org/10.1016/B978-0-12-409548-9.11765-8

Chiang, J. C., & Vimont, D. J. (2004). Analogous Pacific and Atlantic meridional modes of tropical atmosphere-ocean variability. *Journal of Climate*, *17*(21), 4143–4158.

Davey, M., Huddleston, M., Sperber, K., Braconnot, P., Bryan, F., Chen, D., et al. (2002). STOIC: A study of coupled model climatology and variability in tropical ocean regions. *Climate Dynamics*, *18*(5), 403–420.

Eyring, V., Bony, S., Meehl, G. A., Senior, C. A., Stevens, B., Stouffer, R. J., & Taylor, K. E. (2016). Overview of the Coupled Model Intercomparison Project Phase 6 (CMIP6) experimental design and organization. *Geoscientific Model Development*, *9*(5), 1937–1958.

Fang, S.-W., & Yu, J.-Y. (2020). A Control of ENSO transition complexity by tropical Pacific mean SSTs through tropical-subtropical interaction. *Geophysical Research Letters*, *47*, e2020GL087933. https://doi.org/10.1029/2020GL087933

Hu, Z. Z., Kumar, A., Huang, B., Zhu, J., Zhang, R. H., & Jin, F. F. (2017). Asymmetric evolution of El Niño and La Niña: The recharge/discharge processes and role of the off-equatorial sea surface height anomaly. *Climate Dynamics*, *49*(7–8), 2737–2748.

Jin, F. F. (1997). An equatorial ocean recharge paradigm for ENSO. Part I: Conceptual model. *Journal of the Atmospheric Sciences*, *54*(7), 811–829.

Kalnay, E., Kanamitsu, M., Kistler, R., Collins, W., Deaven, D., Gandin, L., et al. (1996). The NCEP/NCAR 40-year reanalysis project. *Bulletin of the American Meteorological Society*, *77*(3), 437–471.
Kao, H. Y., & Yu, J. Y. (2009). Contrasting eastern-Pacific and central-Pacific types of ENSO. *Journal of Climate*, *22*(3), 615–632.
Köhl, A. (2015). Evaluation of the GECCO2 ocean synthesis: Transports of volume, heat and freshwater in the Atlantic. *Quarterly Journal of the Royal Meteorological Society*, *141*(686), 166–181.
Larson, S., & Kirtman, B. (2013). The Pacific meridional mode as a trigger for ENSO in a high-resolution coupled model. *Geophysical Research Letters*, *40*, 3189–3194. https://doi.org/10.1002/grl.50571
Li, G., Xie, S. P., Du, Y., & Luo, Y. (2016). Effects of excessive equatorial cold tongue bias on the projections of tropical Pacific climate change. Part I: The warming pattern in CMIP5 multi-model ensemble. *Climate Dynamics*, *47*(12), 3817–3831.
Lyu, K., Yu, J. Y., & Paek, H. (2017). The influences of the Atlantic multidecadal oscillation on the mean strength of the North Pacific subtropical high during boreal winter. *Journal of Climate*, *30*(1), 411–426.
Misra, V., Marx, L., Brunke, M., & Zeng, X. (2008). The equatorial Pacific cold tongue bias in a coupled climate model. *Journal of Climate*, *21*(22), 5852–5869.
Rayner, N. A., Parker, D. E., Horton, E. B., Folland, C. K., Alexander, L. V., Rowell, D. P., et al. (2003). Global analyses of sea surface temperature, sea ice, and night marine air temperature since the late nineteenth century. *Journal of Geophysical Research*, *108*D14, 4407. https://doi.org/10.1029/2002JD002670
Stuecker, M. F. (2018). Revisiting the Pacific meridional mode. *Scientific Reports*, *8*(1), 1–9.
Suarez, M. J., & Schopf, P. S. (1988). A delayed action oscillator for ENSO. *Journal of the Atmospheric Sciences*, *45*(21), 3283–3287.
Taylor, K. E., Stouffer, R. J., & Meehl, G. A. (2012). An overview of CMIP5 and the experiment design. *Bulletin of the American Meteorological Society*, *93*(4), 485–498.
Timmermann, A., An, S. I., Kug, J. S., Jin, F. F., Cai, W., Capotondi, A., et al. (2018). El Niño-Southern Oscillation complexity. *Nature*, *559*(7715), 535–545. https://doi.org/10.1038/s41586-018-0252-6
Vannière, B., Guilyardi, E., Madec, G., Doblas-Reyes, F. J., & Woolnough, S. (2013). Using seasonal hindcasts to understand the origin of the equatorial cold tongue bias in CGCMs and its impact on ENSO. *Climate Dynamics*, *40*(3–4), 963–981.
Vimont, D. J., Wallace, J. M., & Battisti, D. S. (2003). The seasonal footprinting mechanism in the Pacific: Implications for ENSO. *Journal of Climate*, *16*(16), 2668–2675.
Wang, B., Luo, X., Yang, Y. M., Sun, W., Cane, M. A., Cai, W., et al. (2019). Historical change of El Niño properties sheds light on future changes of extreme El Niño. *Proceedings of the National Academy of Sciences*, *116*(45), 22,512–22,517.
Wang, C., Deser, C., Yu, J. Y., DiNezio, P., & Clement, A. (2017). El Niño and Southern Oscillation (ENSO): A review. In *Coral reefs of the eastern tropical Pacific* (pp. 85–106). Dordrecht: Springer. https://doi.org/10.1007/978-94-017-7499-4_4
Wyrtki, K. (1975). El Niño—The dynamic response of the equatorial Pacific Ocean to atmospheric forcing. *Journal of Physical Oceanography*, *5*(4), 572–584.
Xie, S. P., & Philander, S. G. H. (1994). A coupled ocean-atmosphere model of relevance to the ITCZ in the eastern Pacific. *Tellus A*, *46*(4), 340–350.
Xue, Y., Leetmaa, A., & Ji, M. (2000). ENSO prediction with Markov models: The impact of sea level. *Journal of Climate*, *13*(4), 849–871.
Yu, J.-Y., & Fang, S.-W. (2018). The distinct contributions of the seasonal footprinting and charged-discharged mechanisms to ENSO complexity. *Geophysical Research Letters*, *45*, 6611–6618. https://doi.org/10.1029/2018GL077664
Yu, J. Y., Kao, H. Y., & Lee, T. (2010). Subtropics-related interannual sea surface temperature variability in the central equatorial Pacific. *Journal of Climate*, *23*(11), 2869–2884.
Yu, J.-Y., Wang, X., Yang, S., Paek, H., & Chen, M. (2017). Changing El Niño-Southern Oscillation and associated climate extremes. In S.-Y. Wang, J.-H. Yoon, C. Funk, & R. R. Gillies (Eds.), *Book chapter in Climate extremes: Patterns and mechanisms*, *AGU geophysical monograph series* (Vol. 226, pp. 3–38). Hoboken, NJ: John Wiley & Sons, Inc.
Yu, J. Y., & Kim, S. T. (2011). Relationships between extratropical sea level pressure variations and the central Pacific and eastern Pacific types of ENSO. *Journal of Climate*, *24*(3), 708–720. https://doi.org/10.1175/2010JCLI3688.1
Zebiak, S. E., & Cane, M. A. (1987). A model El Niño-Southern Oscillation. *Monthly Weather Review*, *115*(10), 2262–2278.

*Geophysical Research Letters*

Supporting Information for

# Contrasting transition complexity between El Niño and La Niña: Observations and CMIP5/6 models

Shih-Wei Fang and Jin-Yi Yu

Department of Earth System Science, University of California, Irvine, CA, USA

**Contents of this file**

**Text S1. Methods of calculating the SP-onset and the TP-onset index**

We applied multi-variate empirical orthogonal function (MEOF) analysis to calculate the Subtropical Pacific onset (SP-onset) and the Tropical Pacific onset (TP-onset) indices as in Yu and Fang (2018). MEOF analysis is a statistical method that can identify the dominant coupled processes among multiple fields. In this case, we apply it to capture the ocean-atmosphere coupling processes associated with ENSO, which are manifested by the combined anomalies of sea surface temperatures (SST), surface wind, and sea surface heights (SSH) within the tropical Pacific (20°S–20°N, 122°E–70°W) during the period 1948–2016. The MEOF analysis followed Xue et al. (2000) by applying a two-step empirical orthogonal function (EOF) algorithm. The first step is to apply a spatial EOF analysis separately to the SST, wind, and SSH anomalies to obtain their individual leading EOF modes. The second step is to apply a temporal EOF analysis to the combined principal components (PCs) of the leading spatial EOF modes of each variable. This MEOF yields the leading coupled modes among the SST, wind, and SSH anomalies of the ocean-atmosphere coupling associated with ENSO. The SP-onset and TP-onset index are $2^{nd}$ and $3^{rd}$ leading modes obtained in the observation. The same MEOF analysis was applied to CMIP5/6 model simulations.

**Text S2. Classification of the three types of ENSO transitions**

An El Niño (La Niña) event occurs when the 3-month average of Niño3.4 index (SST anomalies averaged between 5°S-5°N and 170°W-120°W) are larger (smaller) than 0.7 (-0.7) standard deviation for 6 or more consecutive months. The onset and termination of an El Niño (La Niña) event are defined as the months when the averaged Niño3.4 index first goes above or drops below the threshold, respectively. A cyclic ENSO transition is one in which an ENSO event is preceded (within 12 months) by an event of the opposite phase. Similarly, a multi-year ENSO transition is identified the one in which the preceding and the current events are of the same phase. All other transitions are classified as episodic. An event that is longer than 18 months is considered to be two separate events and the second event is identified as a multi-year ENSO event (and additional multi-year events are identified for each additional 12 months that event persists). The effectiveness of this classification method is verified by examining the evolution of the Niño3.4 index (SST anomalies averaged between 5°S-5°N and 170°W-120°W) for each of the transition patterns (see Fig. S1 for the observations, Fig. S2 for CMIP5 models, and Fig. S3 for CMIP6 models).

.

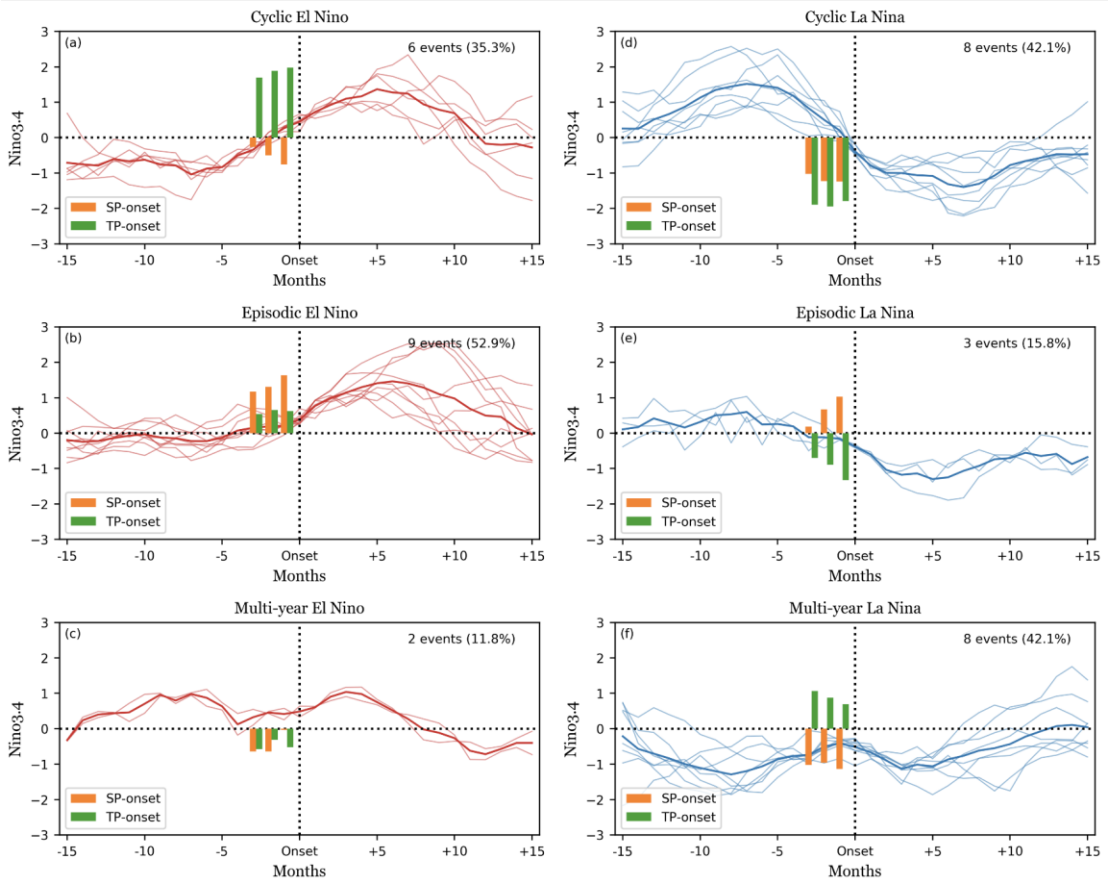


**Figure S1.** Evolutions of the Niño3.4 index during the cyclic, episodic, and multi-year transitions of (a-c) El Niño and (d-f) La Niña. Each thin line represents the evolution of the Niño3.4 index during an individual ENSO event. Thick lines are the mean evolutions of all events in the panel. The evolutions are displayed from 12 months before the ENSO onset month to 12 months after. The mean strengths of the SP-onset index (orange) and TP-onset index (green) during the pre-onset months are shown by the bars for the three months before the ENSO onset month.

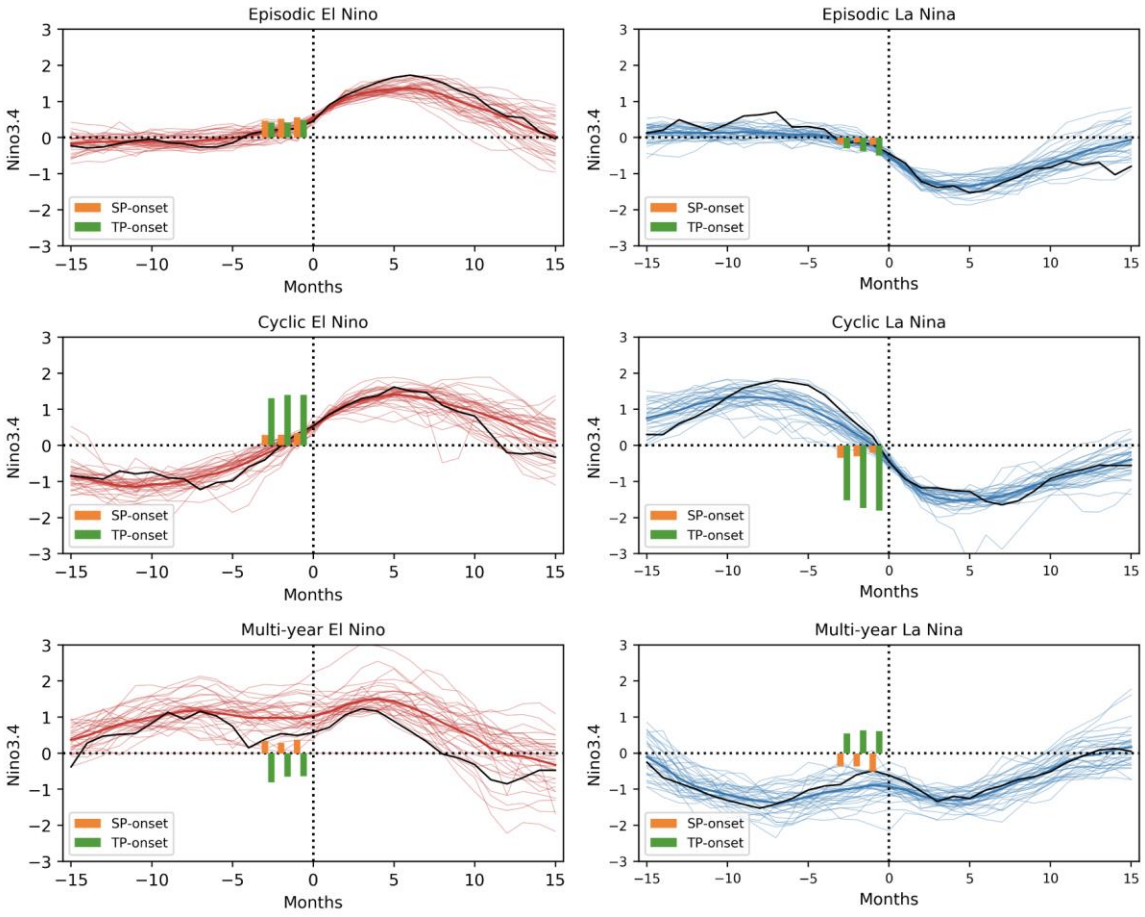


**Figure S2.** Same as Figure S1 but for the CMIP5 models. Thin lines represent the mean evolutions of normalized Niño3.4 index of individual CMIP5 models and the thick line represents their multi-model mean. Black lines are the mean evolutions calculated from the reanalysis. The bars are the multi-model means of the SP-onset index and TP-onset index during the pre-onset months.

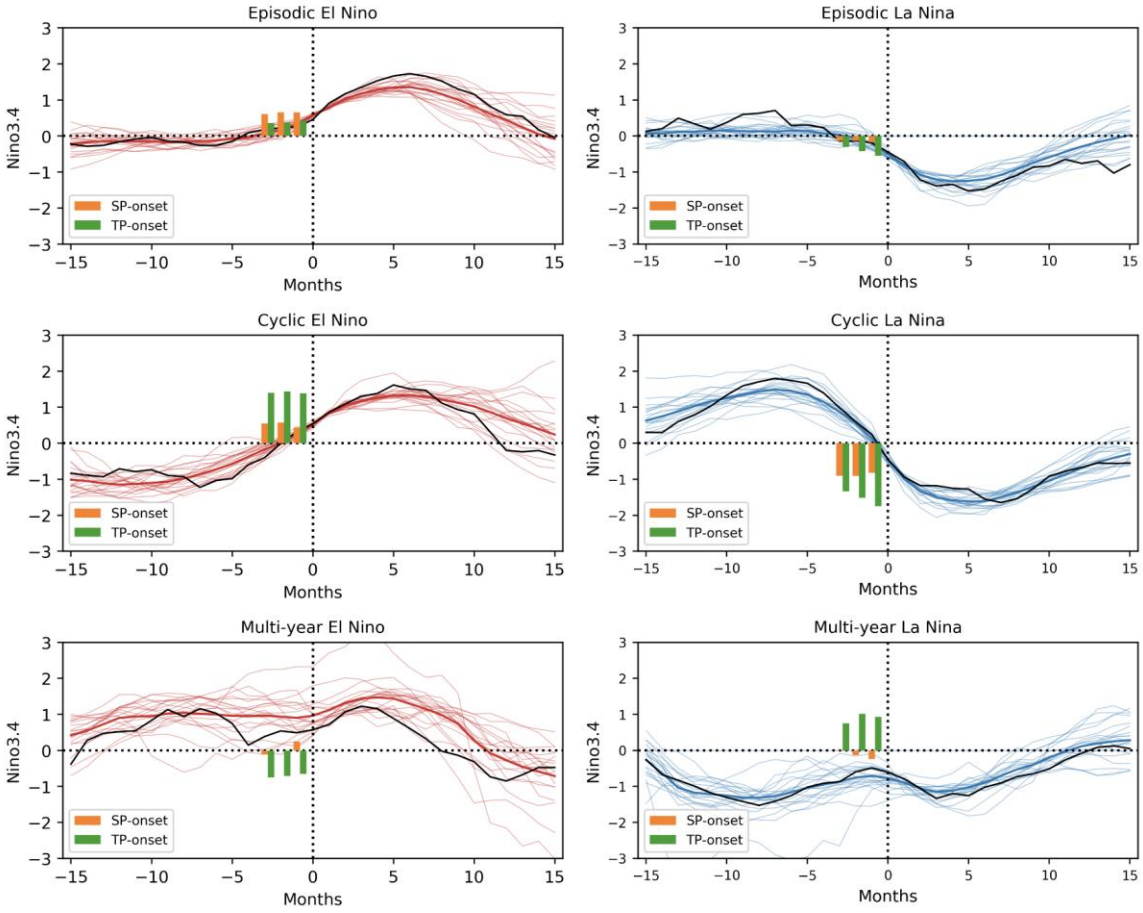


**Figure S3.** As in Figure S2, but for the CMIP6 models.

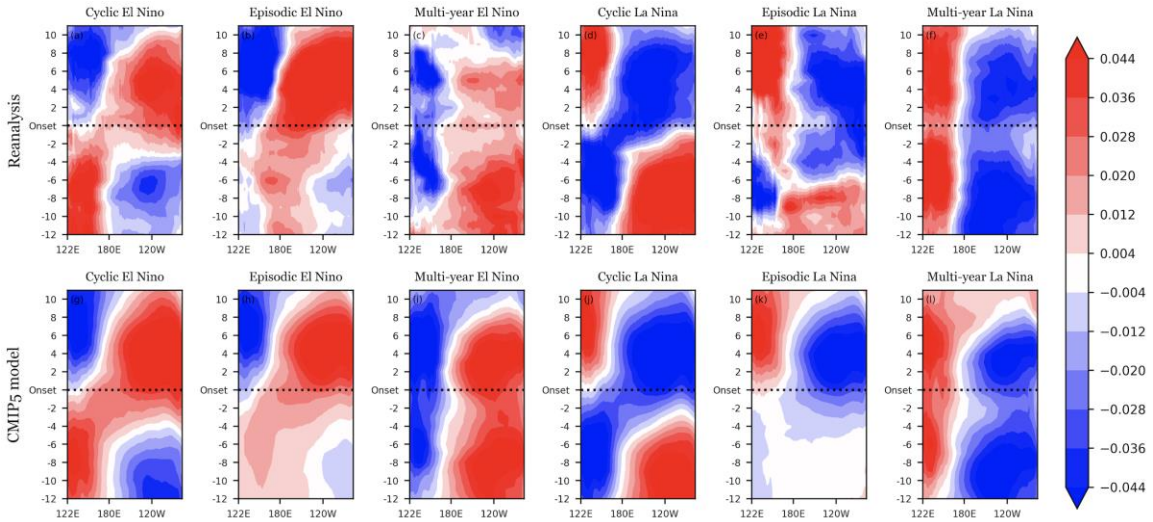


**Figure S4.** As in Figure 2, but for equatorial SSH anomalies (meters).

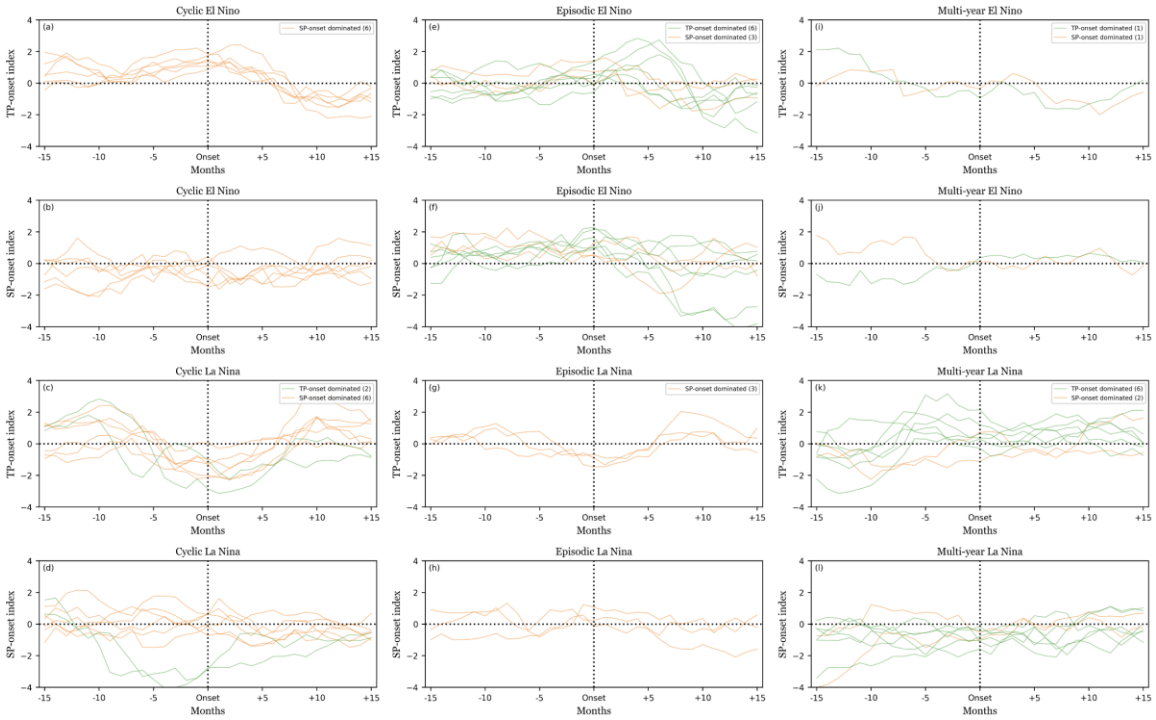


**Figure S5.** The evolution of the normalized TP-onset and SP-onset indices for the three transition patterns of El Niño and La Niña event during the analysis period 1948-2016. Panels (a)-(d) are for the cyclic transition; panels (e)-(h) are for the episodic transition; and panels (i)-(l) are for the multi-year transition. The first row is the TP-onset for El Niño; the second row is the SP-onset for El Niño; the third row is the TP-onset for La Niña; the last row is the SP-onset for La Niña. Each thin line represents the mean evolution of the normalized index and thick lines are the multi-model means. The green lines show transitions that are more associated with the TP-onset mechanism; defined as events where the values of the TP-onset index during the pre-onset months (3 months before the onset months) of El Niño (La Niña) are more positive (negative) than those of the SP-onset index. The orange lines illustrate the transitions that are more associated with the SP-onset mechanism.

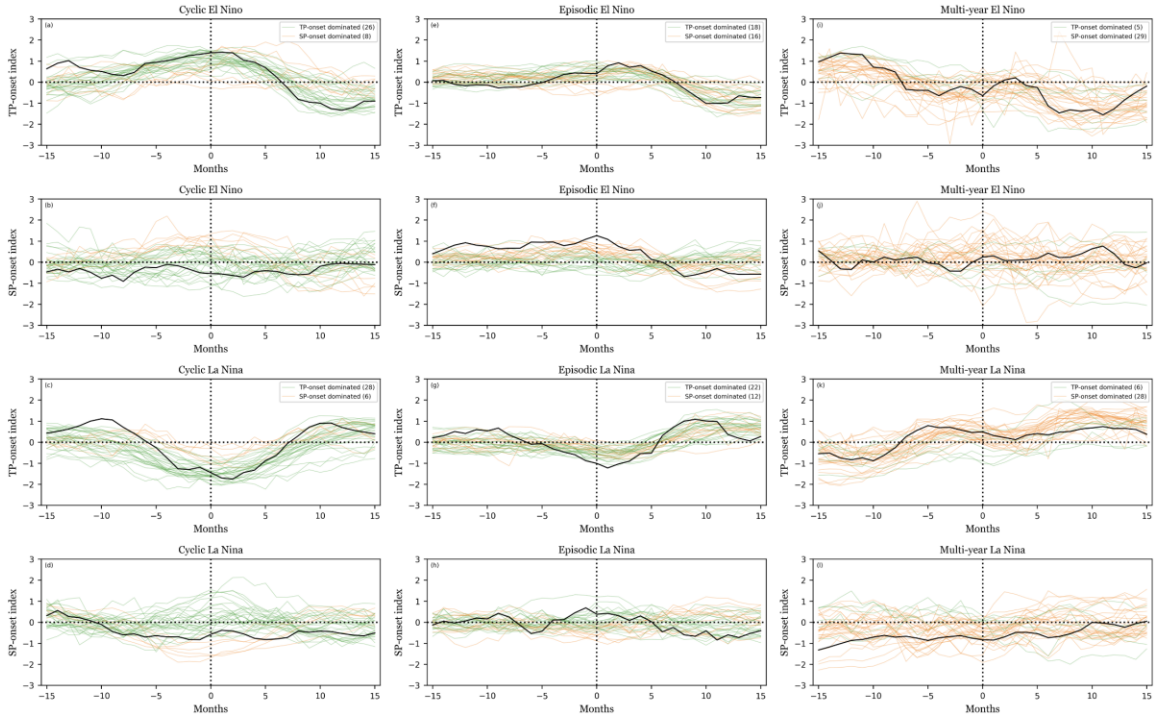


**Figure S6.** As in Figure S5, except the thin lines represent the mean evolutions in the individual CMIP5 models and the thick lines are the multi-model means. The black lines are the mean evolutions for the reanalysis. The green lines show transitions that are more associated with the TP-onset mechanism; defined as event means where the means of the TP-onset indices during the pre-onset months (3 months before the onset months) of El Niño (La Niña) events are more positive (negative) than those of the SP-onset index. The orange lines illustrate the transitions that are more associated with the SP-onset mechanism.

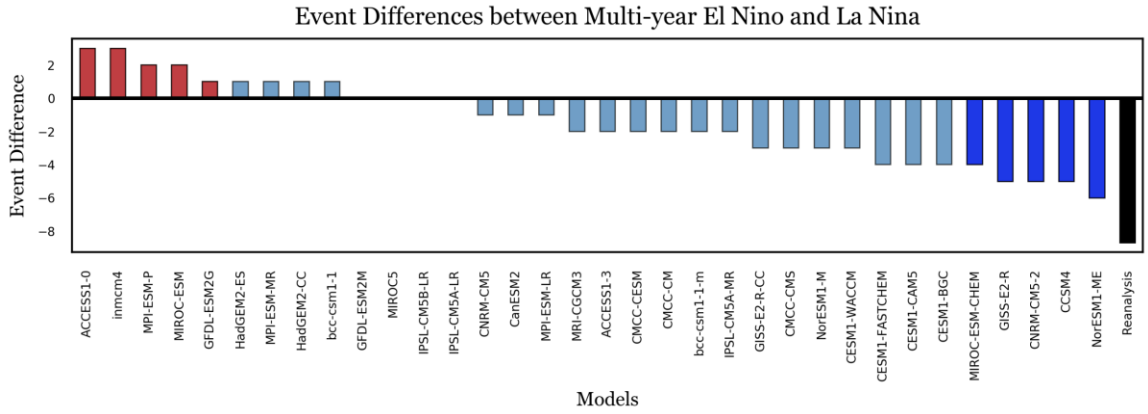


**Figure S7.** The difference in the numbers of multi-year El Niño and multi-year La Niña events. The five models with the largest positive difference (i.e., more multi-year El Niños) are shown in red and the five with the largest negative difference (i.e., more multi-year La Niñas) are shown in blue. The black bar is the reanalysis (scaled to event numbers in 100 years for comparison with 100 year long model simulations).

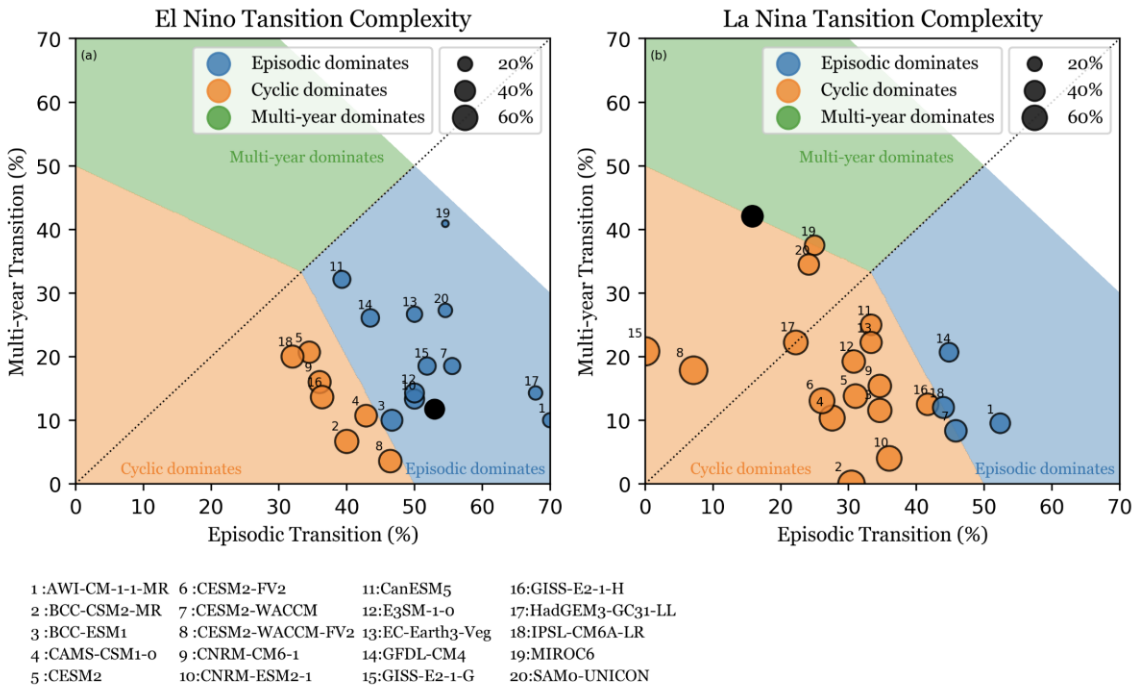


111

112 **Figure S8.** Same as Figure 3 but for 20 CMIP6 model.

113

114

115

116

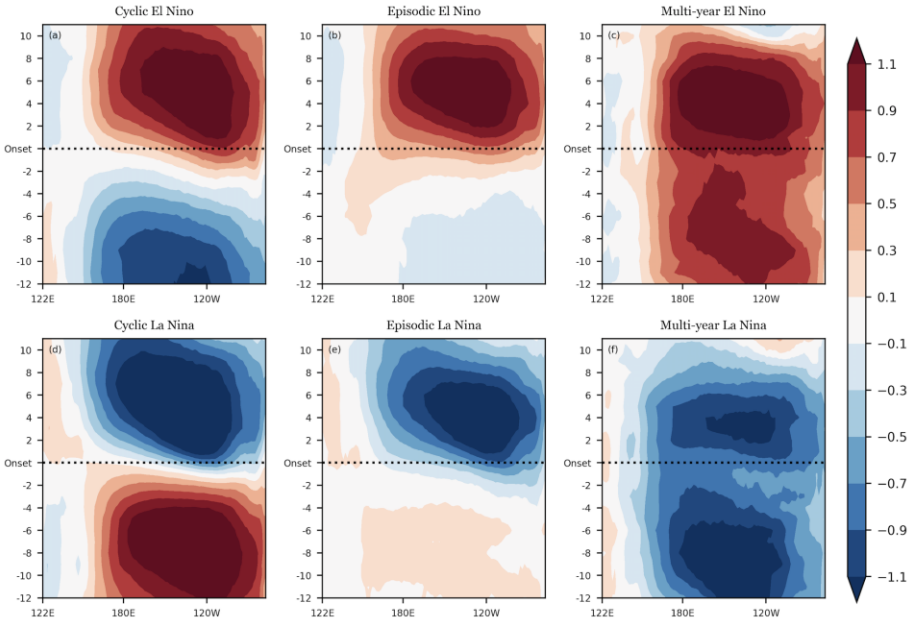


**Figure S9.** As in Fig. 2, except for the CMIP6 models.

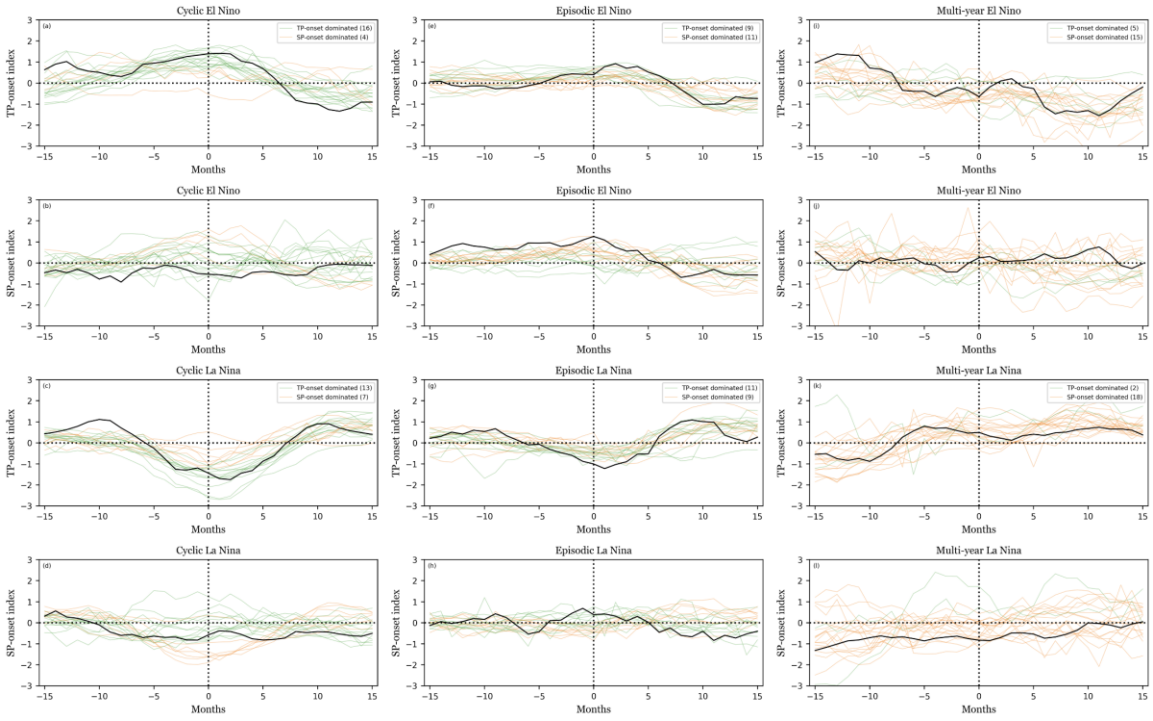


123

124 **Figure S10.** As in Figure S6 but for CMIP6 models.

125

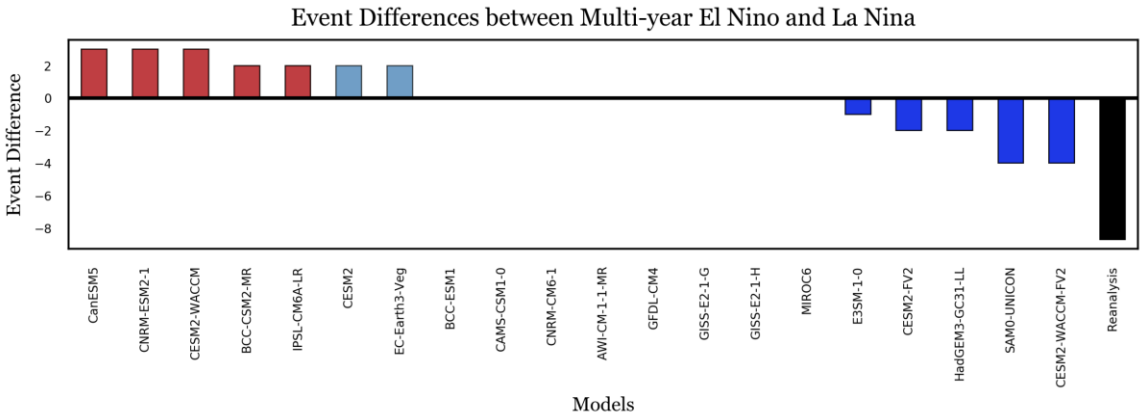


126

127 **Figure S11.** As in Figure S7, except for CMIP6 models.

128

129

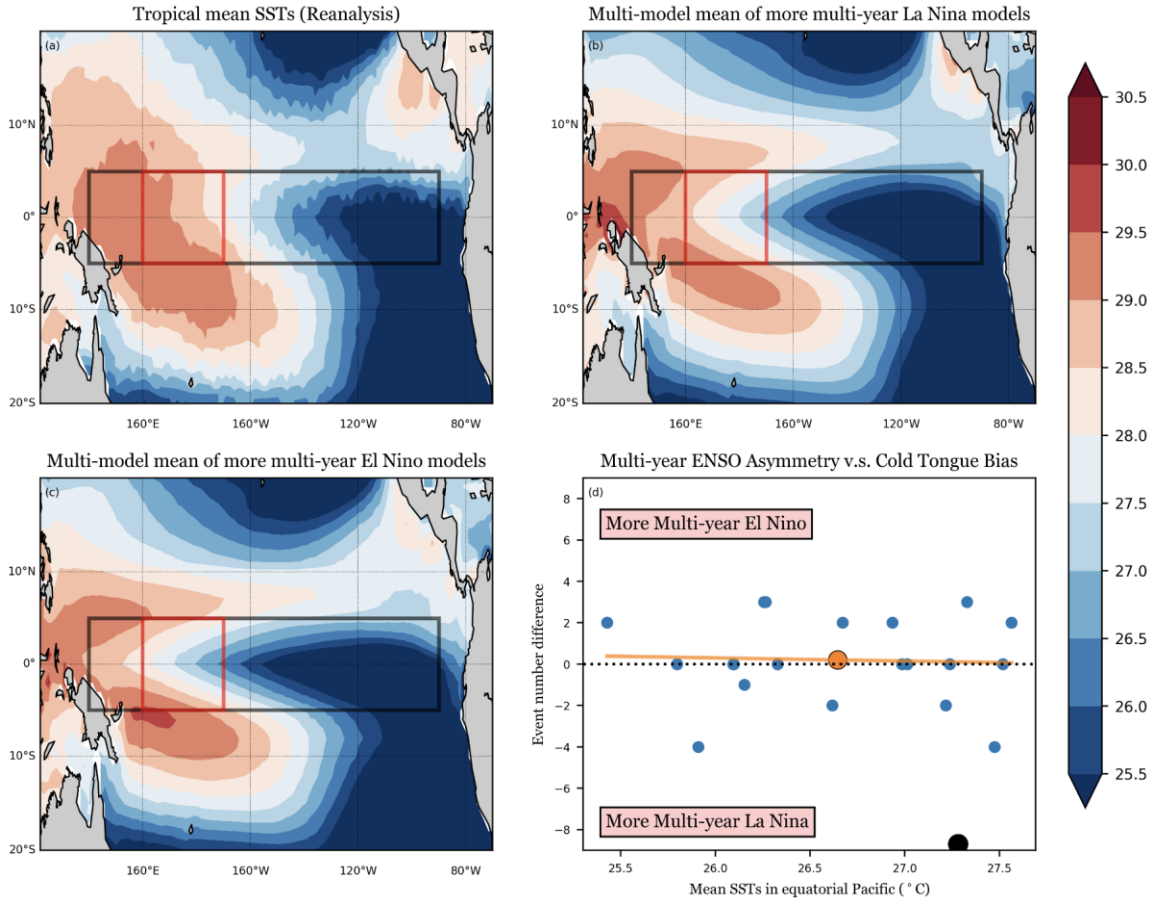


130

131 **Figure S12.** As in Figure 4, except for CMIP6 models.

132

133
134

135

| | Model | Modeling Center | | Model | Modeling Center |
|---|---|---|---|---|---|
| 1 | ACCESS1-0 | Commonwealth Scientific and Industrial Research Organization (CSIRO) and Bureau of Meteorology (BOM), Australia | 18 | HadGEM2-CC | Met Office Hadley Centre |
| 2 | ACCESS1-3 | | 19 | HadGEM2-ES | |
| 3 | CCSM4 | National Center for Atmospheric Research Community Earth System Model Contributors | 20 | IPSL-CM5A-LR | Institut Pierre-Simon Laplace |
| 4 | CESM1-BGC | | 21 | IPSL-CM5A-MR | |
| 5 | CESM1-CAM5 | | 22 | IPSL-CM5B-LR | |
| 6 | CESM1-FASTCHEM | | 23 | MIROC-ESM | Japan Agency for Marine-Earth Science and Technology, Atmosphere and Ocean Research Institute, and National Institute for Environmental Studies |
| 7 | CESM1-WACCM | | 24 | MIROC-ESM-CHEM | |
| 8 | CMCC-CESM | Centro Euro-Mediterraneo per I Cambiamenti Climatici | 25 | MIROC5 | |
| 9 | CMCC-CM | | 26 | MPI-ESM-LR | Max-Planck-Institut für Meteorologie (Max Planck Institute for Meteorology) |
| 10 | CMCC-CMS | | 27 | MPI-ESM-MR | |
| 11 | CNRM-CM5 | Centre National de Recherches Météorologiques | 28 | MPI-ESM-P | |
| 12 | CNRM-CM5-2 | | 29 | MRI-CGCM3 | Meteorological Research Institute |
| 13 | CanESM2 | Canadian Centre for Climate Modelling and Analysis | 30 | NorESM1-M | Norwegian Climate Centre |
| 14 | GFDL-ESM2G | NOAA Geophysical Fluid Dynamics Laboratory | 31 | NorESM1-ME | |
| 15 | GFDL-ESM2M | | 32 | bcc-csm1-1 | Beijing Climate Center, China Meteorological Administration |
| 16 | GISS-E2-R | NASA Goddard Institute for Space Studies | 33 | bcc-csm1-1-m | |
| 17 | GISS-E2-R-CC | | 34 | inmcm4 | Institute for Numerical Mathematics |

136 **Table S1.** The names of the 34 CMIP5 models used in this study.

137
138
139
140

141

| | Model | Modeling Center |
|---|---|---|
| 1 | AWI-CM-1-1-MR | Alfred Wegener Institute, Helmholtz Centre for Polar and Marine Research (AWI), in Bremerhaven |
| 2 | BCC-CSM2-MR | Beijing Climate Center, China Meteorological Administration |
| 3 | BCC-ESM1 | Beijing Climate Center, China Meteorological Administration |
| 4 | CAMS-CSM1-0 | Chinese Academy of Meteorological Sciences |
| 5 | CESM2 | Community Earth System Model Contributors |
| 6 | CESM2-FV2 | |
| 7 | CESM2-WACCM | National Center for Atmospheric Research |
| 8 | CESM2-WACCM-FV2 | |
| 9 | CNRM-CM6-1 | Centre National de Recherches Météorologiques |
| 10 | CNRM-ESM2-1 | |
| 11 | CanESM5 | Canadian Centre for Climate Modelling and Analysis |
| 12 | E3SM-1-0 | U.S. Department of Energy |
| 13 | EC-Earth3-Veg | European EC-Earth consortium |
| 14 | GFDL-CM4 | Geophysical Fluid Dynamics Laboratory |
| 15 | GISS-E2-1-G | NASA Goddard Institute for Space Studies |
| 16 | GISS-E2-1-H | |
| 17 | HadGEM3-GC31-LL | Met Office Hadley Centre |
| 18 | IPSL-CM6A-LR | Institut Pierre-Simon Laplace |
| 19 | MIROC6 | Atmosphere and Ocean Research Institute (The University of Tokyo), National Institute for Environmental Studies, and Japan Agency for Marine-Earth Science and Technology |
| 20 | SAM0-UNICON | Seoul National University |

142 **Table S2.** The names of the 20 CMIP5 models used in this study.

143

144